

Impact of QED radiative corrections on Parton Distribution Functions

Renat R. Sadykov

Joint Institute for Nuclear Research, Joliot-Curie str. 6, Dubna, 141980, Russia

Abstract

The level of precision achieved by the experimental measurements at the LHC requires the inclusion of higher order electroweak effects to the processes of pp scattering. In particular the photon-induced process $\gamma\gamma \rightarrow \ell^+\ell^-$ make a significant contribution ($\sim 10\%$) to the dilepton invariant mass distribution. To evaluate the cross-section of this process one need to know the parton distribution function (PDF) of the photon in the proton $\gamma(x, \mu^2)$. The aim of the current study is to investigate the impact of QED corrections on PDFs and describe the implementation of QED-modified evolution equations into beta release of new version of QCDNUM program. The APPLGRID interface to SANC Monte Carlo generator for fast evaluation of photon-induced cross-section is also outlined. The results were cross-checked with `partonevolution` program, MRST2004QED PDF set and APFEL program. The described developments are planned to include into HERAFitter package and can be used to determine the photon PDF using new data from the LHC experiments.

1 Introduction

With an abundance of high precision measurements available from the LHC experiments, the theoretical precision in matching data accuracy have become crucial. Recent studies on high mass Drell-Yan production in ATLAS [1] have shown that the size of the photon-induced contribution is as large as the uncertainties arising from the different choice of PDF set. Therefore it become important to address the impact of QED corrections to PDFs.

Currently two PDF sets are available which incorporate the photon contribution of the proton. These are old MRST2004QED [2] and most recent NNPDF2.3QED [3].

In this paper an alternative approach is presented. The QED-modified evolution is implemented into beta release of new version of QCDNUM [4] program (v17-01-0b) which allows to solve arbitrary number of coupled DGLAP evolution equations. This implementation together with the APPLGRID [5] interface to SANC [6] Monte Carlo generator for fast evaluation of photon-induced cross-section are planned to include into QCD data fit package HERAFitter [7]. The advantage of this approach is the possibility of using different data sets for QCD fits within a single framework.

The paper is organized as follows. Section 2 describes the modification of QCD evolution required to accommodation for QED effects, section 3 refers to implementation of fast-evaluation of photon-induced process cross-section, in section 4 the comparison of QCDNUM+QED with partonevolution [8] program (v1.1.3), MRST2004QED PDF set and APFEL [9] program (v2.0.0) are presented. Conclusions are given in section 5.

2 QED evolution of parton densities

If the PDFs are known at the initial scale μ_0^2 , then the evaluation of PDFs at the scale μ^2 in pQCD is performed using DGLAP evolution equations. QED-modified DGLAP evolution equations for PDF of quarks $q_i(x, \mu_F^2)$, anti-quarks $\bar{q}_i(x, \mu_F^2)$, gluon $g(x, \mu_F^2)$ and photon $\gamma(x, \mu_F^2)$ can be written as:

$$\begin{aligned}
\frac{\partial q_i}{\partial \ln \mu^2} &= \sum_{j=1}^{n_f} P_{q_i q_j} \otimes q_j + \sum_{j=1}^{n_f} P_{q_i \bar{q}_j} \otimes \bar{q}_j + P_{q_i g} \otimes g + P_{q_i \gamma} \otimes \gamma, \\
\frac{\partial \bar{q}_i}{\partial \ln \mu^2} &= \sum_{j=1}^{n_f} P_{\bar{q}_i q_j} \otimes q_j + \sum_{j=1}^{n_f} P_{\bar{q}_i \bar{q}_j} \otimes \bar{q}_j + P_{\bar{q}_i g} \otimes g + P_{\bar{q}_i \gamma} \otimes \gamma, \\
\frac{\partial g}{\partial \ln \mu^2} &= \sum_{j=1}^{n_f} P_{g q_j} \otimes q_j + \sum_{j=1}^{n_f} P_{g \bar{q}_j} \otimes \bar{q}_j + P_{g g} \otimes g, \\
\frac{\partial \gamma}{\partial \ln \mu^2} &= \sum_{j=1}^{n_f} P_{\gamma q_j} \otimes q_j + \sum_{j=1}^{n_f} P_{\gamma \bar{q}_j} \otimes \bar{q}_j + P_{\gamma \gamma} \otimes \gamma,
\end{aligned} \tag{1}$$

where \otimes -operation denotes the Mellin convolution defined as

$$[f \otimes g](x) \equiv \int_x^1 \frac{dz}{z} f\left(\frac{x}{z}\right) g(z) = \int_x^1 \frac{dz}{z} f(z) g\left(\frac{x}{z}\right). \quad (2)$$

The splitting functions at NLO QCD and LO QED are expressed as

$$\begin{aligned} P_{q_i q_j} &= P_{\bar{q}_i \bar{q}_j} = a_s \delta_{ij} P_{qq}^{(0)} + a_s^2 \left(\delta_{ij} \frac{P_+^{(1)} + P_-^{(1)}}{2} + \frac{P_{qq}^{(1)} - P_+^{(1)}}{2n_f} \right) + a \delta_{ij} e_i e_j \tilde{P}_{qq}^{(0)}, \\ P_{q_i \bar{q}_j} &= P_{\bar{q}_i q_j} = a_s^2 \left(\delta_{ij} \frac{P_+^{(1)} - P_-^{(1)}}{2} + \frac{P_{qq}^{(1)} - P_+^{(1)}}{2n_f} \right), \\ P_{q_i g} &= P_{\bar{q}_i g} = a_s \frac{P_{qg}^{(0)}}{2n_f} + a_s^2 \frac{P_{qg}^{(1)}}{2n_f}, \\ P_{q_i \gamma} &= P_{\bar{q}_i \gamma} = a e_i^2 \frac{P_{q\gamma}^{(0)}}{2n_f}, \\ P_{g q_i} &= P_{g \bar{q}_i} = a_s P_{gq}^{(0)} + a_s^2 P_{gq}^{(1)}, \\ P_{gg} &= a_s P_{gg}^{(0)} + a_s^2 P_{gg}^{(1)}, \\ P_{\gamma q_i} &= P_{\gamma \bar{q}_i} = a e_i^2 P_{\gamma q}^{(0)}, \\ P_{\gamma \gamma} &= a P_{\gamma\gamma}^{(0)}, \end{aligned} \quad (3)$$

where LO splitting kernels are given by

$$\begin{aligned} P_{qq}^{(0)} &= \frac{4}{3} \left(\frac{1+x^2}{(1-x)_+} + \frac{3}{2} \delta(1-x) \right), \quad \tilde{P}_{qq}^{(0)} = \frac{3}{4} P_{qq}^{(0)}, \\ P_{qg}^{(0)} &= n_f (x^2 + (1-x)^2), \quad P_{q\gamma}^{(0)} = 2P_{qg}^{(0)}, \\ P_{gq}^{(0)} &= \frac{4}{3} \left(\frac{1+(1-x)^2}{x} \right), \quad P_{\gamma q}^{(0)} = \frac{3}{4} P_{gq}^{(0)}, \\ P_{gg}^{(0)} &= 6 \left(\frac{x}{(1-x)_+} + \frac{1-x}{x} + x(1-x) + \left(\frac{11}{12} - \frac{n_f}{18} \right) \delta(1-x) \right), \\ \tilde{P}_{\gamma\gamma}^{(0)} &= -\frac{2}{3} \sum_{i=1}^{n_f} e_i^2 \delta(1-x), \end{aligned} \quad (4)$$

and the expressions for NLO singlet splitting kernels $P_{qq}^{(1)}$, $P_{qg}^{(1)}$, $P_{gq}^{(1)}$, $P_{gg}^{(1)}$ can be found in [10] (see footnote on p.9 of [4] concerning the known misprints in these expressions) and those for NLO non-singlet splitting kernels $P_+^{(1)}$, $P_-^{(1)}$ can be found in [11].

For pure QCD evolution the equations (1) can be simplified using singlet and non-singlet combinations of quark densities. Then the singlet quark density obeys the coupled evolution equations with the gluon density and non-singlet combinations evolve independently. This decomposition is not suitable for QED-modified evolution since up- and down- quarks

have different electric charges. Instead for QED evolution we use the following basis of distribution functions:

$$\begin{aligned}
f_1 &= \Delta = u + \bar{u} + c + \bar{c} - d - \bar{d} - s - \bar{s} - b - \bar{b}, \\
f_2 &= \Sigma = u + \bar{u} + c + \bar{c} + d + \bar{d} + s + \bar{s} + b + \bar{b}, \\
f_3 &= g, \\
f_4 &= \gamma, \\
f_5 &= d_v = d - \bar{d}, \\
f_6 &= u_v = u - \bar{u}, \\
f_7 &= \Delta_{ds} = d + \bar{d} - s - \bar{s}, \\
f_8 &= \Delta_{uc} = u + \bar{u} - c - \bar{c}, \\
f_9 &= \Delta_{sb} = s + \bar{s} - b - \bar{b}.
\end{aligned} \tag{5}$$

In this basis we have 4 coupled and 5 uncoupled evolution equations:

$$\begin{aligned}
\frac{\partial}{\partial \ln \mu^2} \begin{pmatrix} f_1 \\ f_2 \\ f_3 \\ f_4 \end{pmatrix} &= \begin{pmatrix} P_{11} & P_{12} & P_{13} & P_{14} \\ P_{21} & P_{22} & P_{23} & P_{24} \\ P_{31} & P_{32} & P_{33} & P_{34} \\ P_{41} & P_{42} & P_{43} & P_{44} \end{pmatrix} \otimes \begin{pmatrix} f_1 \\ f_2 \\ f_3 \\ f_4 \end{pmatrix}, \\
\frac{\partial f_i}{\partial \ln \mu^2} &= P_{ii} \otimes f_i, \quad i = 5, \dots, 9.
\end{aligned} \tag{6}$$

We find after simple calculations that the expressions for splitting kernels P_{ii} in this basis are given by

$$\begin{aligned}
P_{11} &= a_s P_{qq}^{(0)} + a_s^2 P_+^{(1)} + \frac{e_u^2 + e_d^2}{2} a \tilde{P}_{qq}^{(0)}, & P_{33} &= a_s P_{gg}^{(0)} + a_s^2 P_{gg}^{(1)}, \\
P_{12} &= \frac{n_u - n_d}{n_f} a_s^2 (P_{qq}^{(1)} - P_+^{(1)}) + \frac{e_u^2 - e_d^2}{2} a \tilde{P}_{qq}^{(0)}, & P_{34} &= 0, \\
P_{13} &= \frac{n_u - n_d}{n_f} (a_s P_{qg}^{(0)} + a_s^2 P_{qg}^{(1)}), & P_{41} &= \frac{e_u^2 - e_d^2}{2} a P_{\gamma q}^{(0)}, \\
P_{14} &= \frac{n_u e_u^2 - n_d e_d^2}{n_f} a P_{q\gamma}^{(0)}, & P_{42} &= \frac{e_u^2 + e_d^2}{2} a P_{\gamma q}^{(0)}, \\
P_{21} &= \frac{e_u^2 - e_d^2}{2} a \tilde{P}_{qq}^{(0)}, & P_{43} &= 0, \\
P_{22} &= a_s P_{qq}^{(0)} + a_s^2 P_{qq}^{(1)} + \frac{e_u^2 + e_d^2}{2} a \tilde{P}_{qq}^{(0)}, & P_{44} &= a P_{\gamma\gamma}^{(0)}, \\
P_{23} &= a_s P_{qg}^{(0)} + a_s^2 P_{qg}^{(1)}, & P_{55} &= a_s P_{qq}^{(0)} + a_s^2 P_-^{(1)} + a e_d^2 \tilde{P}_{qq}^{(0)}, \\
P_{24} &= \frac{n_u e_u^2 + n_d e_d^2}{n_f} a P_{q\gamma}^{(0)}, & P_{66} &= a_s P_{qq}^{(0)} + a_s^2 P_-^{(1)} + a e_u^2 \tilde{P}_{qq}^{(0)}, \\
P_{31} &= 0, & P_{77} &= P_{99} = a_s P_{qq}^{(0)} + a_s^2 P_+^{(1)} + a e_d^2 \tilde{P}_{qq}^{(0)}, \\
P_{32} &= a_s P_{gq}^{(0)} + a_s^2 P_{gq}^{(1)}, & P_{88} &= a_s P_{qq}^{(0)} + a_s^2 P_+^{(1)} + a e_u^2 \tilde{P}_{qq}^{(0)}.
\end{aligned} \tag{7}$$

The new beta version of QCDNUM program has routines to solve arbitrary number of coupled evolution equations and is therefore suitable for solving of equations (6). The flavour decomposition (5) and the splitting kernels (7) were implemented into user module of this version of QCDNUM.

3 Photon-induced process

Corrections to the neutral current Drell-Yan cross-section due to photon-induced process $\gamma\gamma \rightarrow \ell^+\ell^-$ can reach up to 10 – 20% for high invariant mass $M_{\ell^+\ell^-}$ with the appropriate choice of kinematic cuts [12]. Therefore it is important to use this contribution for data fits when extracting photon PDF from LHC data.

3-differential cross-section of the process $p[\gamma]p[\gamma] \rightarrow \ell^+\ell^-$ at LO reads

$$\begin{aligned} \frac{d\sigma(p[\gamma]p[\gamma] \rightarrow \ell^+\ell^-)}{dx dy dz} &= \\ &= \frac{4\pi\alpha^2}{s_0} f_\gamma\left(\frac{M_{min}}{\sqrt{s_0}}e^{x+y}, \mu_F^2\right) f_\gamma\left(\frac{M_{min}}{\sqrt{s_0}}e^{x-y}, \mu_F^2\right) (1 + \tanh^2 z), \\ x &= \ln \frac{M_{\ell^+\ell^-}}{M_{min}}, \quad y = Y_{\ell^+\ell^-}, \quad z = -\ln \tan \frac{\theta}{2}. \end{aligned} \quad (8)$$

For fast evaluation of this cross-section the **APPLGRID** interface to the **SANC** Monte Carlo generator was created. The interface is organized as follows:

- **SANC** generator produces unweighted events which are saved to data file. Each event i is assigned a weight

$$w_i = \frac{\sigma_{tot}}{N} \cdot \frac{1}{f_\gamma(x_{1i}, \mu_i^2) f_\gamma(x_{2i}, \mu_i^2)},$$

where $\sigma_{tot} = \int d\sigma$ is the total cross-section and N is total number of generated events. **MRST2004QED** PDF set is used to evaluate the photon PDF.

- These events are used to fill grids for different observables with help of **APPLGRID** interface.
- These grids then can be used for fast convolution with arbitrary photon PDF to get the cross-section.

The standard **APPLGRID** package was modified so one can handle one extra PDF (photon) in addition to 13 standard PDFs (gluon and quarks).

4 Validation and performance

The described implementation of QED-modified DGLAP evolution equations (which we denote as **QCDNUM+QED**) was cross-checked with **partonevolution** program in fixed flavour number scheme (FFNS) and with **MRST2004QED** PDF set and **APFEL** program in variable flavour number scheme (VFNS). It takes ~ 5 s of CPU time (Intel Core i7-3630QM, 2.4 GHz) to fill weight tables of splitting functions and ~ 0.5 s to evolve the distributions (5) on 100×100 grid in x and μ^2 .

4.1 Comparison of QCDNUM+QED and partonevolution

For the numerical comparison of QCDNUM+QED and partonevolution (PE) codes the toy model with $n_f = 4$ is adopted. PDFs at initial scale $\mu_0 = 2$ GeV are given by:

$$\begin{aligned}
xu_v &= \frac{35}{16}x^{0.5}(1-x)^3, \\
xd_v &= \frac{315}{256}x^{0.5}(1-x)^4, \\
x\bar{d} = x\bar{u} = x\bar{s} = xs &= \frac{0.673345}{6}x^{-0.2}(1-x)^7, \\
x\bar{c} = xc &= 0, \\
xg &= 1.90836x^{-0.2}(1-x)^5, \\
x\gamma &= 0.
\end{aligned} \tag{9}$$

The running strong $a_s = \alpha_s/2\pi$ and electromagnetic $a = \alpha/2\pi$ couplings determined by the following expressions:

$$\begin{aligned}
a_s(\mu^2) &= \frac{1}{\beta_0 L} \left(1 - \frac{\beta_1}{\beta_0^2} \frac{\ln L}{L} \right), \\
a(\mu^2) &= \frac{a(m_\tau^2)}{1 - \frac{38}{9}a(m_\tau^2) \ln \frac{\mu^2}{m_\tau^2}},
\end{aligned} \tag{10}$$

where

$$\begin{aligned}
L &= \ln \frac{\mu^2}{\Lambda_{QCD}^2}, \quad \Lambda_{QCD} = 0.25 \text{ GeV}, \quad \beta_0 = \frac{25}{6}, \quad \beta_1 = \frac{77}{6}, \\
a(m_\tau^2) &= \frac{1}{2\pi} \frac{1}{133.4}, \quad m_\tau = 1.777 \text{ GeV}.
\end{aligned} \tag{11}$$

The results of comparison in FFNS for basis distributions (5) are presented in Figs. 1-8 for momentum distributions xf and the corresponding relative differences which are defined by

$$\delta f = \frac{xf(\text{QCDNUM+QED}) - xf(\text{PE})}{xf(\text{PE})}. \tag{12}$$

A very good agreement is observed between two codes. For photon distribution there is about 1 – 2% difference which can be explained by the effect of contribution from lepton PDFs that are taken into account in PE code. The discontinuity around $x = 0.033$ in the δf plot for Δ distribution is due to the Δ distribution changes sign from - to + near this point.

4.2 Comparison of QCDNUM+QED and MRST2004QED

To compare QCDNUM+QED with MRST2004QED PDF the starting distributions were taken at initial scale $\mu_0 = 2$ GeV using LHAPDF interface. Then this distributions were evolved to the scale $\mu = 100$ GeV on 1000×1000 grid in x and μ^2 . The results of comparison in VFNS for momentum distributions xf and the corresponding relative differences

$$\delta f = \frac{xf(\text{QCDNUM+QED}) - xf(\text{MRST2004QED})}{xf(\text{MRST2004QED})} \quad (13)$$

are presented in Figs. 9-17 where an agreement within $\sim 1\%$ is observed excluding a region of x where PDFs are very small.

4.3 Comparison of QCDNUM+QED and APFEL

For the numerical comparison of QCDNUM+QED and APFEL in VFNS the distributions were evolved from initial scale $\mu_0 = 2$ GeV to $\mu = 100$ GeV on 1000×1000 grid in x and μ^2 . The parametrization for initial PDFs were taken from [13]. The results of comparison in VFNS for momentum distributions xf and the corresponding relative differences

$$\delta f = \frac{xf(\text{QCDNUM+QED}) - xf(\text{APFEL})}{xf(\text{APFEL})} \quad (14)$$

are presented in Figs. 18-26 where an agreement within $\sim 1\%$ is observed excluding a region of large x . A larger discrepancy for photon distribution can be caused by different treatment of $\mathcal{O}(\alpha^2)$ effects.

5 Conclusions

QED-modified evolution equations are implemented into beta version of the next release of QCDNUM program and cross-checked with `partonevolution` program in FFNS and with MRST2004QED PDF set and APFEL program in VFNS. The APPLGRID interface to SANC Monte Carlo generator was created for fast evaluation of LO photon-induced cross-section. These developments are planned to implement into HERAFitter package and can be used for QED fits of LHC data.

Acknowledgements

I would like to thank the HERAFitter team and the ATLAS group in DESY for kind hospitality. I am grateful to M. Botje for helpful discussions of the features of new QCDNUM version and to R. Placakyte and V. Radescu for their comments on the paper draft. This work are supported in part by BMBF-JINR cooperation program and RFBR grant 12-02-91526-IJEPH_a.

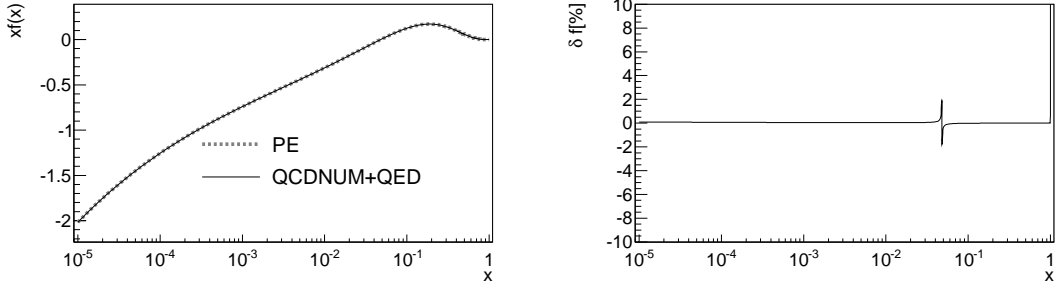


Figure 1: Tuned comparison between QCDNUM+QED and partonevolution. Left plot shows the momentum distribution of Δ at $\mu^2 = 10^4 \text{ GeV}^2$. The corresponding δf is shown on the right plot.

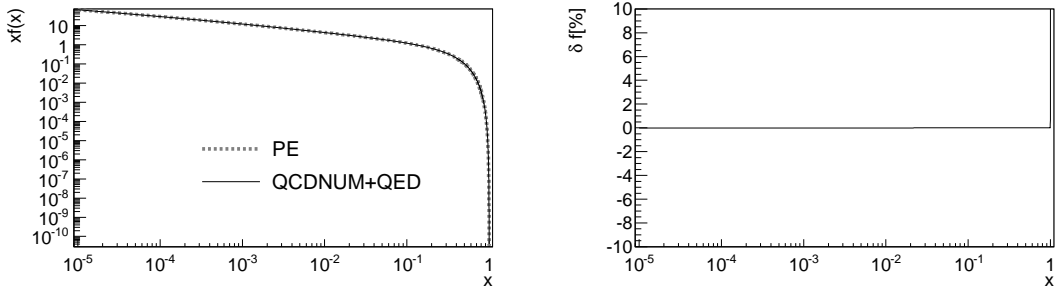


Figure 2: Tuned comparison between QCDNUM+QED and partonevolution. Left plot shows the momentum distribution of Σ at $\mu^2 = 10^4 \text{ GeV}^2$. The corresponding δf is shown on the right plot.

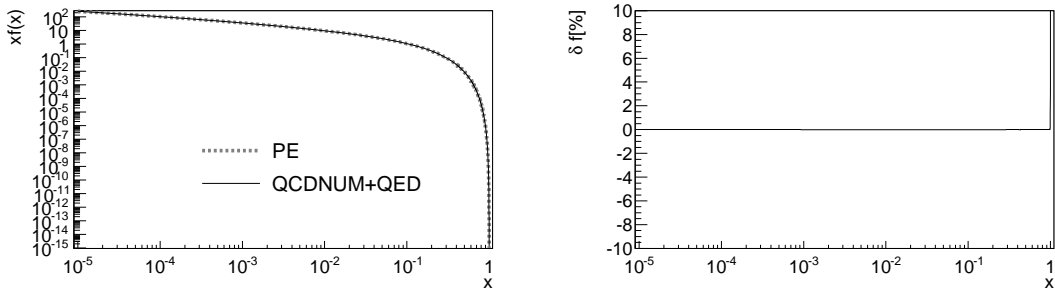


Figure 3: Tuned comparison between QCDNUM+QED and partonevolution. Left plot shows the momentum distribution of g at $\mu^2 = 10^4 \text{ GeV}^2$. The corresponding δf is shown on the right plot.

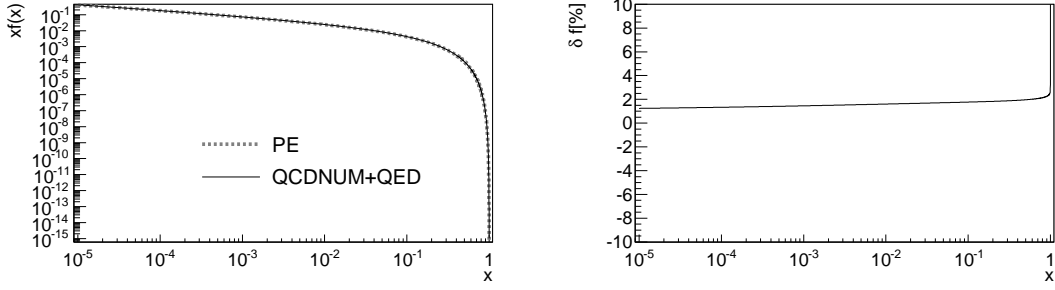


Figure 4: Tuned comparison between QCDNUM+QED and partonevolution. Left plot shows the momentum distribution of γ at $\mu^2 = 10^4 \text{ GeV}^2$. The corresponding δf is shown on the right plot.

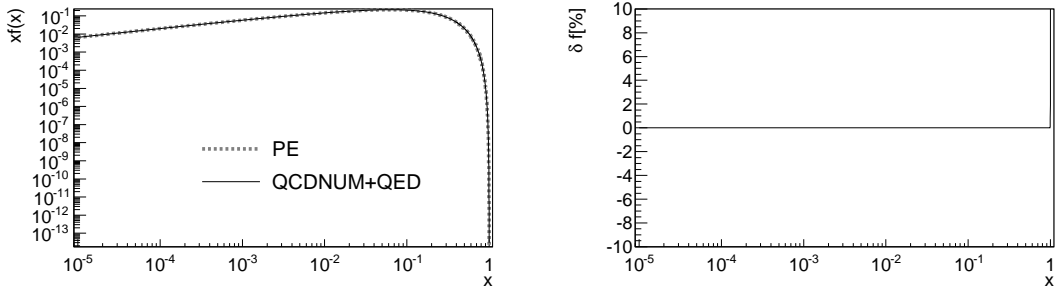


Figure 5: Tuned comparison between QCDNUM+QED and partonevolution. Left plot shows the momentum distribution of d_v at $\mu^2 = 10^4 \text{ GeV}^2$. The corresponding δf is shown on the right plot.

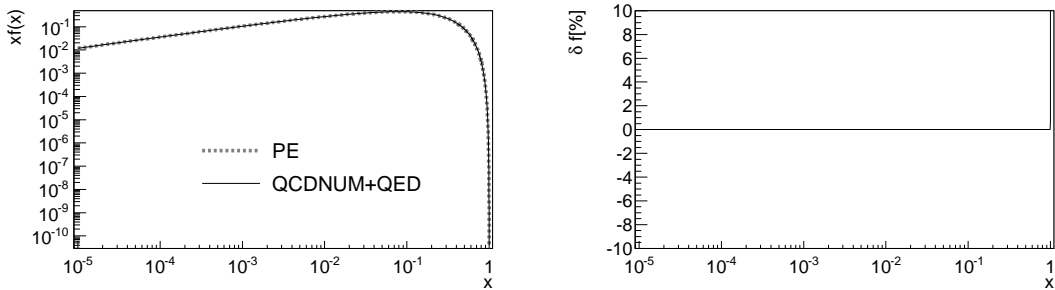


Figure 6: Tuned comparison between QCDNUM+QED and partonevolution. Left plot shows the momentum distribution of u_v at $\mu^2 = 10^4 \text{ GeV}^2$. The corresponding δf is shown on the right plot.

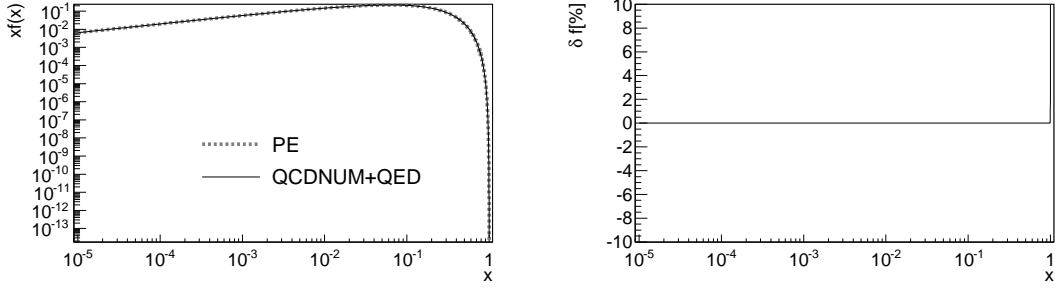


Figure 7: Tuned comparison between QCDNUM+QED and partonevolution. Left plot shows the momentum distribution of Δ_{ds} at $\mu^2 = 10^4 \text{ GeV}^2$. The corresponding δf is shown on the right plot.

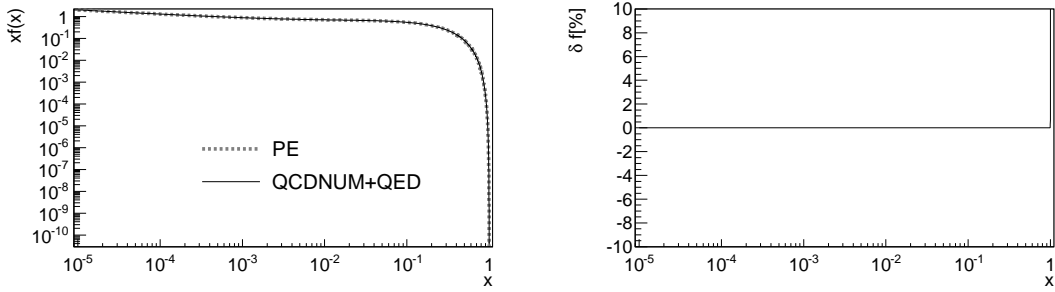


Figure 8: Tuned comparison between QCDNUM+QED and partonevolution. Left plot shows the momentum distribution of Δ_{uc} at $\mu^2 = 10^4 \text{ GeV}^2$. The corresponding δf is shown on the right plot.

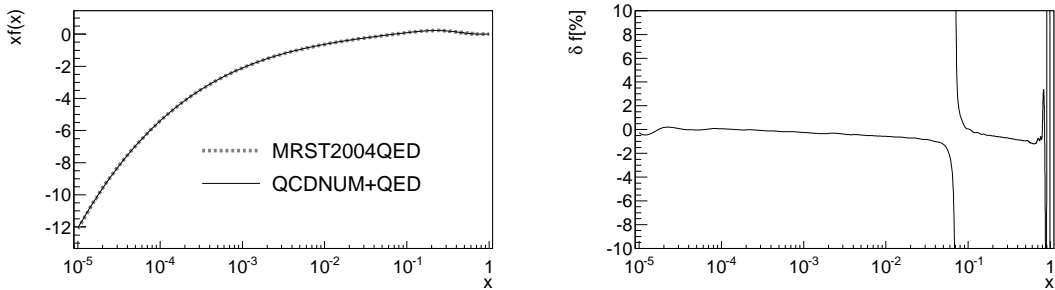


Figure 9: Tuned comparison between QCDNUM+QED and MRST2004QED. Left plot shows the momentum distribution of Δ at $\mu^2 = 10^4 \text{ GeV}^2$. The corresponding δf is shown on the right plot.

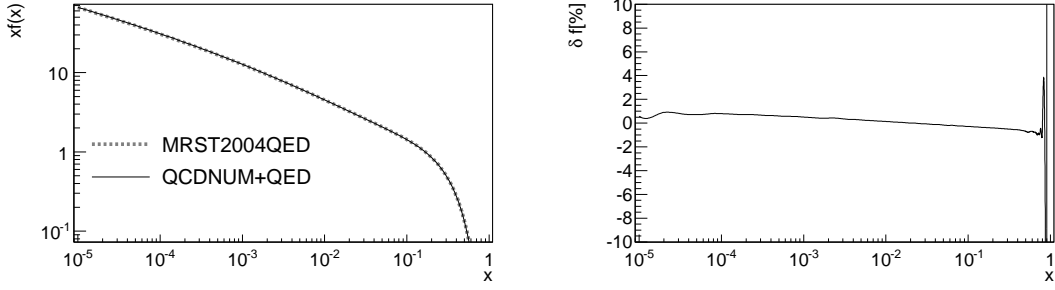


Figure 10: Tuned comparison between QCDNUM+QED and MRST2004QED. Left plot shows the momentum distribution of Σ at $\mu^2 = 10^4 \text{ GeV}^2$. The corresponding δf is shown on the right plot.

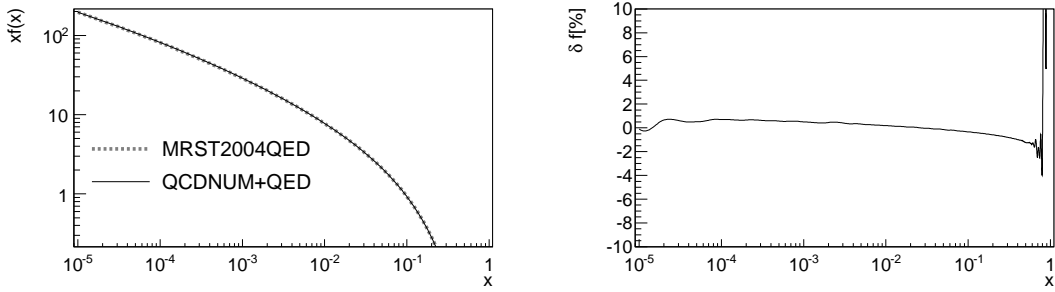


Figure 11: Tuned comparison between QCDNUM+QED and MRST2004QED. Left plot shows the momentum distribution of g at $\mu^2 = 10^4 \text{ GeV}^2$. The corresponding δf is shown on the right plot.

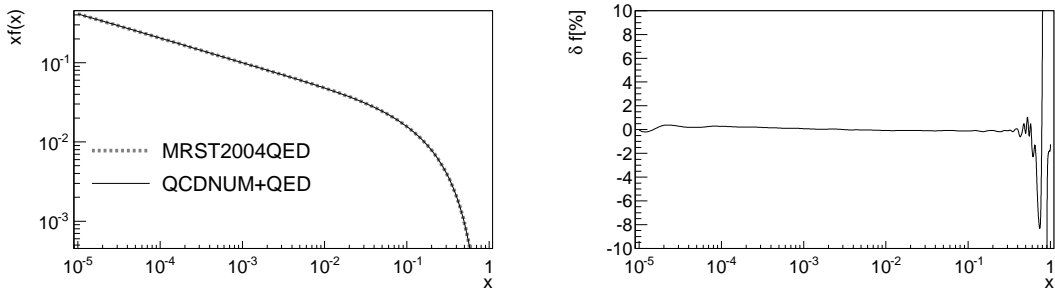


Figure 12: Tuned comparison between QCDNUM+QED and MRST2004QED. Left plot shows the momentum distribution of γ at $\mu^2 = 10^4 \text{ GeV}^2$. The corresponding δf is shown on the right plot.

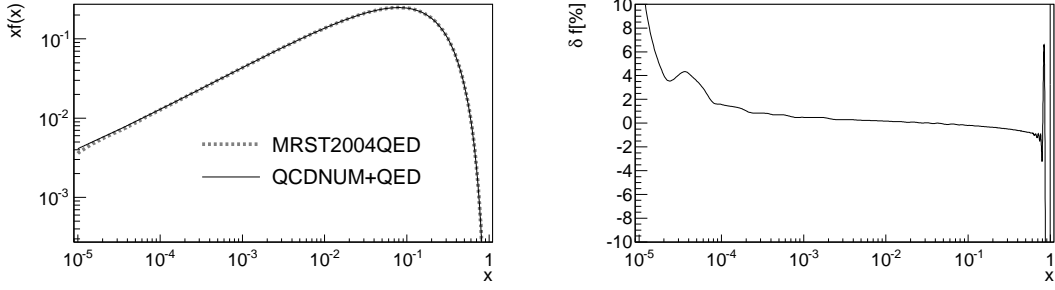


Figure 13: Tuned comparison between QCDNUM+QED and MRST2004QED. Left plot shows the momentum distribution of d_v at $\mu^2 = 10^4 \text{ GeV}^2$. The corresponding δf is shown on the right plot.

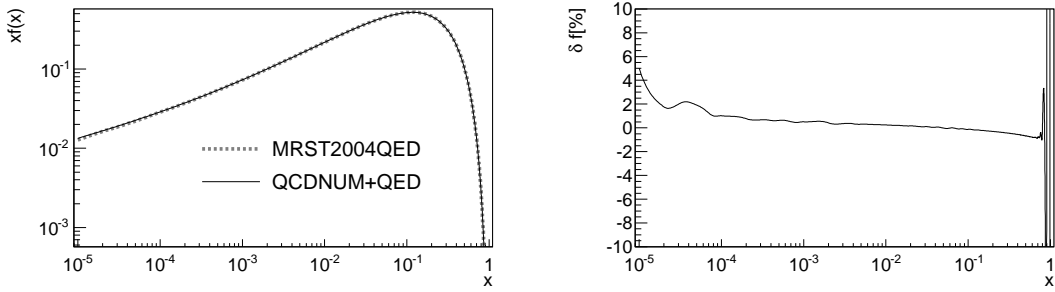


Figure 14: Tuned comparison between QCDNUM+QED and MRST2004QED. Left plot shows the momentum distribution of u_v at $\mu^2 = 10^4 \text{ GeV}^2$. The corresponding δf is shown on the right plot.

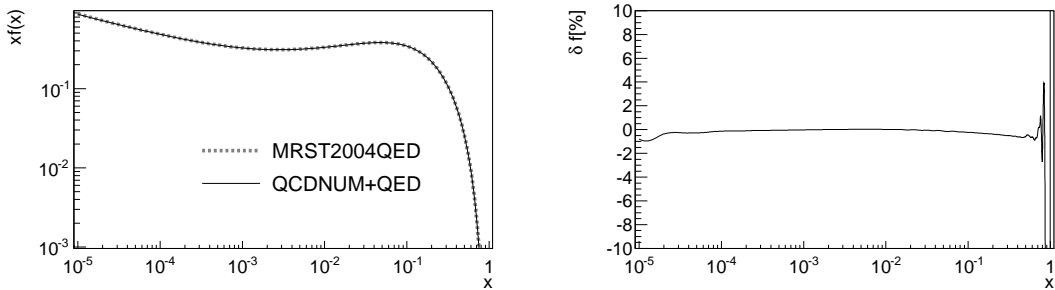


Figure 15: Tuned comparison between QCDNUM+QED and MRST2004QED. Left plot shows the momentum distribution of Δ_{ds} at $\mu^2 = 10^4 \text{ GeV}^2$. The corresponding δf is shown on the right plot.

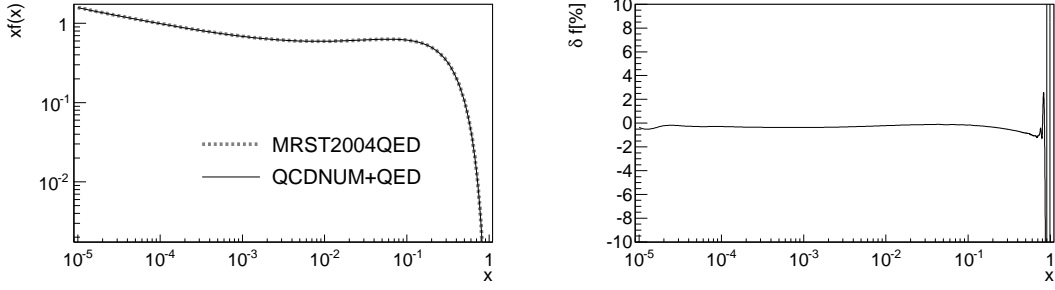


Figure 16: Tuned comparison between QCDNUM+QED and MRST2004QED. Left plot shows the momentum distribution of Δ_{uc} at $\mu^2 = 10^4 \text{ GeV}^2$. The corresponding δf is shown on the right plot.

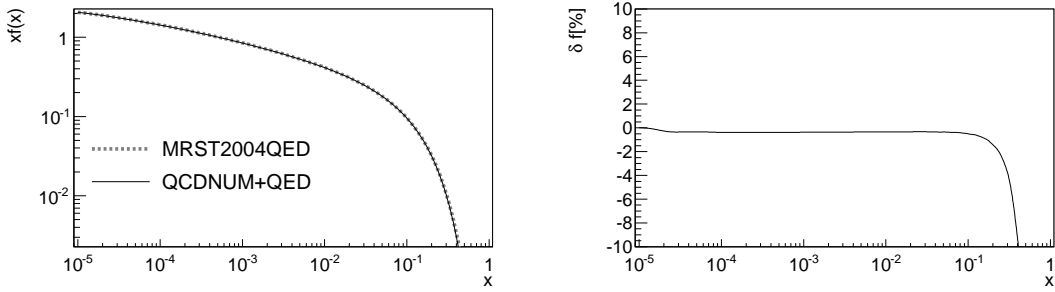


Figure 17: Tuned comparison between QCDNUM+QED and MRST2004QED. Left plot shows the momentum distribution of Δ_{sb} at $\mu^2 = 10^4 \text{ GeV}^2$. The corresponding δf is shown on the right plot.

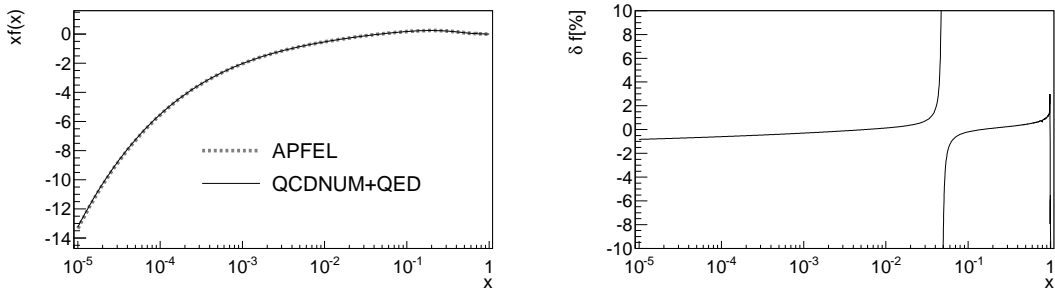


Figure 18: Tuned comparison between QCDNUM+QED and APFEL. Left plot shows the momentum distribution of Δ at $\mu^2 = 10^4 \text{ GeV}^2$. The corresponding δf is shown on the right plot.

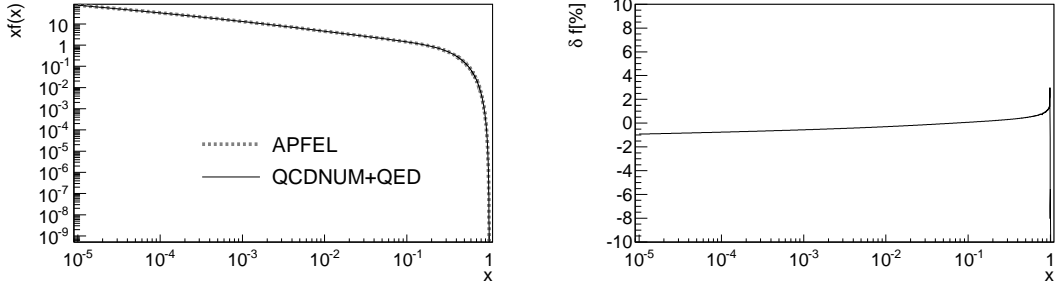


Figure 19: Tuned comparison between QCDNUM+QED and APFEL. Left plot shows the momentum distribution of Σ at $\mu^2 = 10^4 \text{ GeV}^2$. The corresponding δf is shown on the right plot.

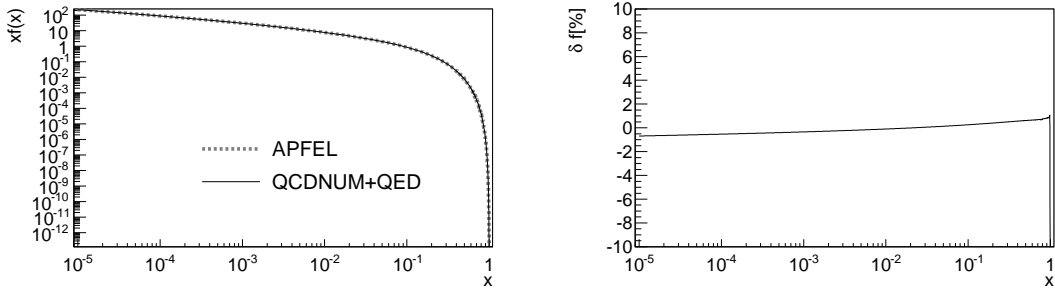


Figure 20: Tuned comparison between QCDNUM+QED and APFEL. Left plot shows the momentum distribution of g at $\mu^2 = 10^4 \text{ GeV}^2$. The corresponding δf is shown on the right plot.

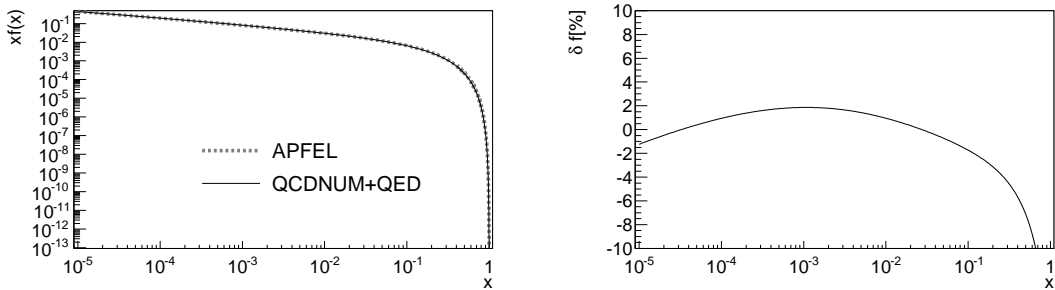


Figure 21: Tuned comparison between QCDNUM+QED and APFEL. Left plot shows the momentum distribution of γ at $\mu^2 = 10^4 \text{ GeV}^2$. The corresponding δf is shown on the right plot.

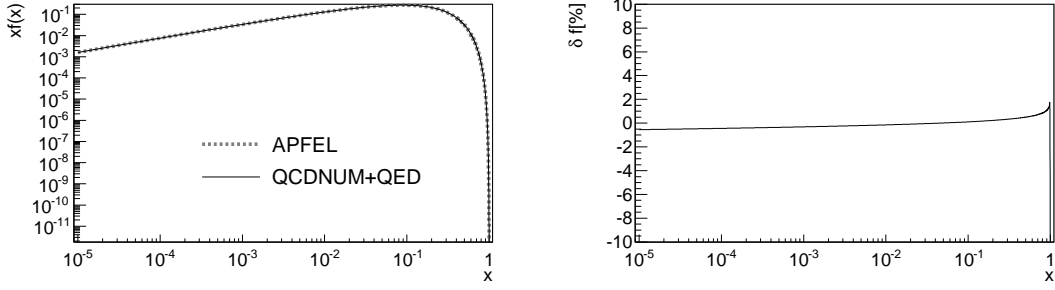


Figure 22: Tuned comparison between QCDNUM+QED and APFEL. Left plot shows the momentum distribution of d_v at $\mu^2 = 10^4 \text{ GeV}^2$. The corresponding δf is shown on the right plot.

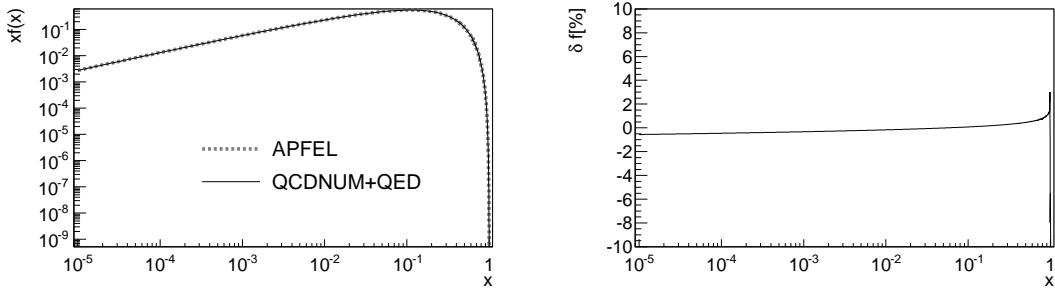


Figure 23: Tuned comparison between QCDNUM+QED and APFEL. Left plot shows the momentum distribution of u_v at $\mu^2 = 10^4 \text{ GeV}^2$. The corresponding δf is shown on the right plot.

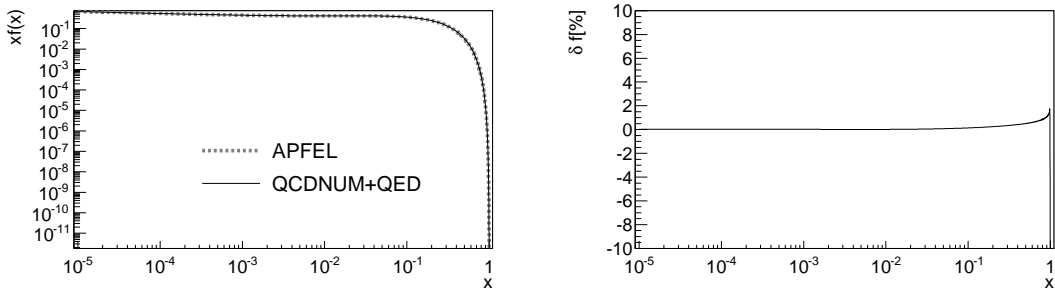


Figure 24: Tuned comparison between QCDNUM+QED and APFEL. Left plot shows the momentum distribution of Δ_{ds} at $\mu^2 = 10^4 \text{ GeV}^2$. The corresponding δf is shown on the right plot.

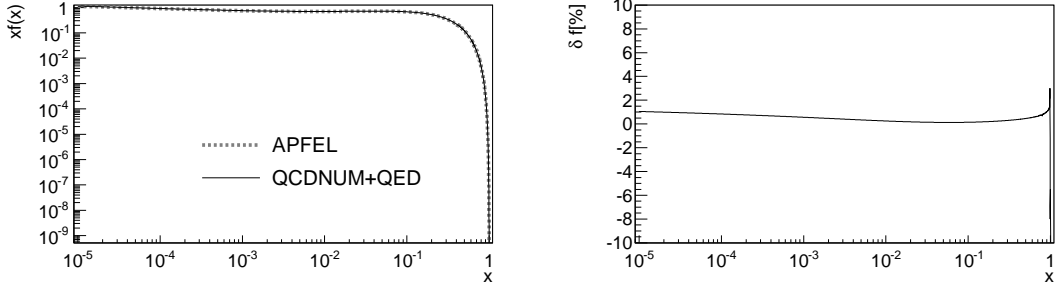


Figure 25: Tuned comparison between QCDNUM+QED and APFEL. Left plot shows the momentum distribution of Δ_{uc} at $\mu^2 = 10^4$ GeV². The corresponding δf is shown on the right plot.

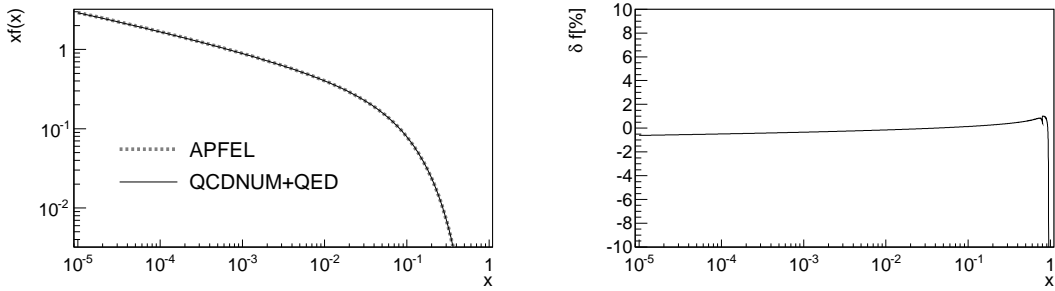


Figure 26: Tuned comparison between QCDNUM+QED and APFEL. Left plot shows the momentum distribution of Δ_{sb} at $\mu^2 = 10^4$ GeV². The corresponding δf is shown on the right plot.

References

- [1] G. Aad *et al.* [ATLAS Collaboration], Phys. Lett. B **725**, 223 (2013) [arXiv:1305.4192 [hep-ex]].
- [2] A. D. Martin, R. G. Roberts, W. J. Stirling and R. S. Thorne, Eur. Phys. J. C **39**, 155 (2005) [hep-ph/0411040].
- [3] R. D. Ball *et al.* [The NNPDF Collaboration], arXiv:1308.0598 [hep-ph].
- [4] M. Botje, Comput. Phys. Commun. **182**, 490 (2011) [arXiv:1005.1481 [hep-ph]].
- [5] M. Sutton, T. Carli, D. Clements, A. Cooper-Sarkar, C. Gwenlan, G. P. Salam, F. Siegert and P. Starovoitov, PoS DIS **2010**, 051 (2010).

- [6] A. Andonov, A. Arbuzov, D. Bardin, S. Bondarenko, P. Christova, L. Kalinovskaya, V. Kolesnikov and R. Sadykov, Comput. Phys. Commun. **181**, 305 (2010) [arXiv:0812.4207 [physics.comp-ph]].
- [7] H. Abramowicz *et al.* [H1 and ZEUS Collaborations], Eur. Phys. J. C **73**, 2311 (2013) [arXiv:1211.1182 [hep-ex]].
- [8] S. Weinzierl, Comput. Phys. Commun. **148**, 314 (2002) [hep-ph/0203112].
- [9] V. Bertone, S. Carrazza and J. Rojo, arXiv:1310.1394 [hep-ph].
- [10] W. Furmanski and R. Petronzio, Phys. Lett. B **97**, 437 (1980).
- [11] G. Curci, W. Furmanski and R. Petronzio, Nucl. Phys. B **175**, 27 (1980).
- [12] S. Dittmaier and M. Huber, JHEP **1001**, 060 (2010) [arXiv:0911.2329 [hep-ph]].
- [13] W. Giele, E. W. N. Glover, I. Hinchliffe, J. Huston, E. Laenen, E. Pilon, A. Vogt and S. Alekhin *et al.*, hep-ph/0204316.